Gigantic effect due to phase transition on thermoelectric properties of ionic sol-gel materials

Jin Liu[1,2], Wei Zeng[3], Xiaoming Tao*[1,2]
[1] Research Institute for Intelligent Wearable Systems
[2]Institute of Textiles and Clothing
The Hong Kong Polytechnic University, Hong Kong China
[3]The Center of Flexible Sensing Technology, Institute of Chemical Engineering,
Guangdong Academy of Sciences, Guangzhou 510665, China
xiao-ming.tao@polyu.edu.hk

Abstract

Sol-gel phase transition in ionic thermoelectrical (i-TE) materials induces large rapid change in viscosity and ionic transport process thus it is expected to give a drastic variation in thermoelectric properties, crucial in low-grade waste heat harvesting for Internet of thing (IoT) and wearable electronic applications. In this work, we prepare and examine four types of ionic thermoelectric materials featured with non-phase-transition, thermal sol-to-gel phase-transition, thermal gel-to-sol phase-transition and UV-induced sol-to-gel phase-transition. For the first time, we observe a large rise of the thermopower by 6.5 times during the sol-gel transition of poloxamer/LiCl system, an even greater ionic figure of merit by around 23 times. The phenomenon is found to be universal as the large variation in thermopower is confirmed in the other thermal gel-sol transitional and UV induced transitional materials. We further reveal the mechanism and propose a model that deals with the pre-, post- and during- phase-transition processes. Finally, we probe six factors influencing the huge variation of the thermopower during the phase-transition and shed light on the possible gigantic changes of thermopower during the phase transition. We uncover a possible route to design and control the desired TE performances of materials, which can lead to a new sight in tunable i-TE devices for low-heat energy harvesting applications.

Keywords: ionic thermoelectric materials, phase-transition, thermopower, model, design and control of thermoelectric properties.

1. Introduction

With the explosive growth of flexible, light-weighted and wearable electronics and

Internet of Things (IoT), the usage of IoT nodes and sensors has quickly approached the predicted trillion pieces.[1,2] However, the lack of efficient, light-weighted and environmental friendly power sources has been the bottleneck that hinders the wide applications of IoT and wearable technologies.[3] One of the attractive solutions is the use of solid-state thermoelectric generators (TEGs), which can directly convert waste heat from environment or human body into electricity without any moving parts.[4,5]

Both electronic and ionic thermoelectric materials have been explored as candidates for TEGs. Researchers use a dimensionless figure of merit ($ZT=\sigma S^2T/\kappa$, where σ is the electrical conductivity, S the Seebeck coefficient, κ the thermal conductivity, and T the absolute temperature) to describe the conversion efficiency. Electronic thermoelectric materials are mainly narrow band-gap semiconductors, which have widely been studied and used where either electrons or holes act as the charge carriers. Group IV and VI compounds, such as PbTe, SnTe and SnSe, or other metallic crystal compoundes, such as Cu_2Se are often widely studied electronic thermoelectric materials.[6–11] However, the Seebeck coefficient of these materials are normally quite low (around 200-400 $\mu V/K$)[12], which means the generation of a useful voltage (several volts) near room temperature requires either an integration of thousands of tiny TE cells[13] or a DC-DC voltage booster which both increase the complexity in device or fabrication process.[14] In addition, due to the strong inter-relations between the Seebeck coefficient, electrical conductivity and thermal conductivity,[15,16] manipulation of any single parameter in order to improve the overall thermoelectric performances, especially the ZT value, becomes a challenge. Therefore, researchers tried to discover many methods such as band convergence, band flattening or density of states distortion to optimizing the thermoelectric performances.[8,17,18]

Alternatively, different from the electronic thermoelectric systems, ionic thermoelectric (i-TE) systems use cations and anions as charge carriers and driven by either thermodiffusion effect or thermogalvanic effect, which make them possess a thermopower, or ionic Seebeck coefficient, a few orders of magnitude higher than that of the conventional semiconductor materials at room temperature.[19,20] For instance, 1 mV/K at room temperature[21] was shown from a simple aqueous solution of salt like LiCl or NaCl while 11 mV/K was obtained by using NaOH in a polyethylene oxide (PEO) solution.[19] In order to overcome the difficulty in encapsulation[22], quasi-solid-state electrolytes have been demonstrated as solid i-TE materials for applications. A thermopower of 24 mV/K, two orders of magnitude higher than that of electronic semiconductor TE materials, was achieved by using NaOH-PEO aqueous solution in confined nanocelluosic channels.[23] In addition, an adjustable thermopower from -4

mV/K to 14 mV/K was reported by tailoring the composition of polymer gel.[24] However, the ZT values of such quasi-solid-state i-TE materials are normally less than 0.1 because of their poor electrical conductivity. Recently, ionic gels made of ionic liquids and poly(vinylidene fluoride-co-hexafluoropropylene) (PVDF-HFP) show a thermopower up to 26.1 mV/K together with an ionic conductivity of 6.7 mS/cm, which makes a high ZT value of 0.75.[21] The high thermopower of i-TE materials is attribute to the Soret effect of ions, which causes the accumulations of the ions at the different ends of the system.[25] The thermopower of the i-TE system, especially the thermodiffusive cells, is determined by the concentration differences between the cations and anions at both hot and cold ends. Therefore, the transportation process of the ions is critical for high performance of the quasi-solid i-TE material systems.

Previous works have focused on ion species or ion chemical effects to improve the thermoelectric performances of the i-TE materials. However, the environment of the transportations of ions, the electrolytes, also plays an important role. The use of electrolyte permits electrically control of electronic, magnetic and optical properties of materials [26] and phase-transition induced electrochemical performances in aqueous hybrid-ion batteries.[27] The sol-to-gel or vise-visa phase-transition can change the viscosity due to formation or destruction of polymer network, therefore we stipulate that the phase transition would have a significant impact on the transportation process thus the thermopower of i-TE materials.

In this work, we prepare and investigate the effect of phase transition in four i-TE materials with different phase-transitional behavior and mechanism, that is, the four materials featured with non-phase-transition, thermal sol-to-gel phase-transition, thermal gel-to-sol phase-transition and UV-induced sol-to-gel phase-transition, respectively. We report a discovery of a 6.5-fold and 23-fold increment of the thermopower and ionic figure of merit (ZT_i), respectively, during the thermal sol-gel phase transition in a poloxamer/LiCl aqueous i-TE material. We also observe that the large drop of thermopower during the gel-sol transition in an agarose/LiCl system and big rise in thermopower during the phase transition induced by cross-linking due to UV irradiation of an epoxy/LiCl system. In order to reveal the operational mechanism, we propose a semi-quantitative model covering the pre-, post- and during-transition stages, by using Onsager relations and Eastman's theory.[25] The model derives the thermopower change during the phase-transition as a function of six dimensionless parameters. We then probe the six influencing factors and confirm the very possibility for gigantic increment in thermopower during a phase-transition of i-TE system. Based on the theoretical analysis and experimental observation, we speculate that this phase-

transition-induced thermopower phenomenon is universal regardless the type of causes for the sol-gel phase transition and confirm it by rise of thermopower in the epoxy/LiCl system during the phase-transition caused by UV irradiation. The study, for the first time, reveals a universal phenomenon of huge variation caused by the phase-transition in i-TE systems and its mechanism, sheds light on a novel and feasible venue to improve energy conversion performance of i-TE materials by controlled phase-transition, which may lead to a new perspective for future tunable i-TE devices for low-heat energy harvesting applications.

2. Results and discussion

In this project, all the i-TE materials exhibit in non-solid forms, which means we need to build test cells to examine the properties. **Figure 1a** and **1b** show the components of the i-TE materials and the test cells, respectively. The details about the preparation of the i-TE materials and test cells will be illustrated in the experimental section and **Figure S1**.

2.1 I-TE Materials: The poloxamer 407 aqueous solutions exhibit a sol-to-gel phase transition at room temperature within a concentration between 15% (w/v) to 20% (w/v).[28] We observed this by pouring the poloxamer solutions into a test tube and tested the liquid surface layer by declining the test tube at different temperature (**Figure 1c**). At low temperature, the solution is in liquid-state and the surface layer keeps horizontal when obliqued. At high temperature, the solution is in gel-state and the surface layer keeps the same shape with its initial state when obliqued. Then we confirmed the phase transition by the plot of viscosity vs. temperature (**Figure 1d(i)**). The concentration of electrolytes required for the phase transition was determined at which a rapid change of viscosity occurred at the sol-gel phase transition. The result shows the sol-to-gel transition temperature decreases as the concentration of the poloxamer 407 increases, which indicates aqueous solution with higher concentration can form a gel-state at lower temperature. This thermogelation can result from the interactions between different segments of the polymer.[29] As the temperature increases, the hydrophobic PO blocks in the polymer start to dehydrate and the molecules tend to form spherical structures. The gel-state will then form by ordered pack of the sufficient concentrated samples. Therefore, the higher concentration can improve the gelation process which result in the lower temperature requirements for the thermogelation process.

We investigated the non-transitional or pre-transitional i-TE systems at first. As shown in **Figure S2**, the thermopower of the solution with 1 mol/L LiCl and 10% (w/v) poloxamer 407, is around 2-3 mV/K at room temperature and appears independent on

the temperature. At this low concentration, the solution almost experienced no phase-transition and maintained the liquid-state at room temperature. This value is quite low compared with other works and is compatible with the thermopower of the thermogalvanic cells.[30–32] i-TE systems consist of poloxamer and other ions from various salts (e.g. NaCl, KCl, $NaNO_3$) investigated by us show similar results to that of the LiCl poloxamer system (**Figure S2**).

Then we studied transitional i-TE material systems. Poloxamer 407 aqueous solutions with higher concentration and varied molality of the Li ions were explored. Limited by the solubility of the salt and capability of phase-transition, the suitable molality of the ions in this work was found to be 1 mol/L. In addition, the concentration of the poloxamer 407 solution was controlled between 15 – 20% (w/v) to fulfill the requirements of sol-gel phase-transition under room temperature. Therefore, we selected the 1 mol/L LiCl with 18% (w/v) poloxamer 407 solution as target and picked 1 mol/L LiCl with 20% (w/v) poloxamer 407 solution for comparison.

2.2 Thermopower in transitional i-TE materials: By changing the temperature at the cold side from 5℃ to 35℃, the measured thermopower of the ionic system varies from 2 mV/K to more than 15 mV/K (**Figure 1e**). The thermopower of the ionic system reaches a maximum of around 15.4 mV/K at around 17.4 ℃, when the i-TE system changes from the liquid-state to gel-state (**Figure 1d(ii)**). Below the phase transition temperature, the ionic system behaves as a homogenous liquid and the thermopower of the system is quite low (around 2-3 mV/K), which is similar to the thermopower of the non-transitional ionic system with 10 % (w/v) poloxamer 407. Above the transition, the i-TE system acts as a homogenous hydrogel and the thermopower of the gel system is also quite low (around 2-3 mV/K), which is similar to that of the liquid system. The thermopower of the ionic system seems to not have an obvious difference in homogenous liquid-state and gel-state and is likely to have no dependence on the concentration of the poloxamer 407 solution. Therefore, the huge enhancement (6.5 folds) of the thermopower of the ionic system during the phase-transition may be due to the transport changes of ions in different states of the electrolytes. To further confirm this finding, we selected a similar i-TE system but with increased concentration of the poloxamer 407 solution, which can adjust the temperature range of the phase-transition. **Figure 1f** shows the relations between the thermopower and temperature in the i-TE system with 20% (w/v) poloxamer. Similarly, the thermopower of the 20% (w/v) poloxamer system shows a peak value of around 9.8 mV/K at around 16.9 ℃, which is also the phase-transition temperature for this system (**Figure 1d(ii)**).

One may ask if it is possible to reverse the change direction and induce a huge reduction in thermopower of a transitional i-TE system? To answer this question, we prepared another kind of ionic system by using 1 mol/L LiCl with 2% (w/v) Agarose aqueous solution. Like poloxamer 407, the agarose aqueous solution experiences a gel-sol phase transition when the temperature rises. The agarose aqueous solution is in gel-state below the transition temperature but in sol-state above it, which is opposite to the direction of sol-gel phase-transition process of poloxamer 407.[33] **Figure 1g** shows the relationships between the thermopower and temperature of the agarose-based ionic system. It is evident that a sudden drop of the thermopower occurs when the temperature is around 30 ℃, which is also around the phase-transition temperature of the material (**Figure 1d(iii)**).

2.3 Thermal, electrical conductivity and ZT values: We measured the electrical and thermal conductivity of the 1 mol/L LiCl/18% (w/v) poloxamer 407 i-TE system to derive the output power and ZT values. **Figure 1h** shows the near room-temperature ionic electrical conductivity of the i-TE system. Traditional methods to measure the electrical conductivity of solid TE semiconductors cannot be applied to liquid-state materials. Therefore, we measured the electrical impedance first and derived the electrical conductivity was calculated from the real part of the impedance from the measurement results from near zero phase angle region. The electrical conductivity of the i-TE system almost has no temperature dependency and the phase-transition does not display any effect on the electrical conductivity, which may be because the working mode of this i-TE system is capacitance mode (**Figure S4-S5**). **Figure 1i** shows the measured near- room-temperature thermal conductivity of the i-TE system. It is quite close to the value of pure water (0.5 W/(m·K)) and has no obvious temperature dependency. Therefore, the thermopower of the i-TE is the major factor to affect the TE performances with changing temperature. Based on the ionic electrical conductivity, thermopower and thermal conductivity, we can calculate ZT_i to describe the converting efficiency of the i-TE cell (**Figure 1j**). Similar with the figure of merit (ZT) in traditional electronic thermoelectric generator (TEG), ionic figure of merit can be defined as $ZT_i = S^2\sigma T/\kappa$, where S, σ and κ represent the thermopower, ionic electrical conductivity and thermal conductivity, respectively. However, the i-TE materials with the same ZT value of the classic TEGs should have lower efficiency.[34] This is because that the i-TE cells in this project works in capacitance mode and output power is decrease with time. Nevertheless, ZT_i should also be an important factor to describe the efficiency of the i-TE materials.[35] We can observe a sudden increment of around 23 folds (less than 0.03 to 0.68) at the phase-transition temperature of the i-TE material. In addition, by using the formula from previous research, we can also calculate the

maximum converting efficiency of the i-TE cells increase from 3.08×10^{-5} to around 6.18×10^{-4} (more than 20 times) during phase transition.[34]

2.4 Mechanisms: The thermodiffusive thermopower is defined as $S = -\frac{V(T_H)-V(T_C)}{\Delta T}$, where $V(T_H)$ and $V(T_C)$ represent the voltage at the hot temperature T_H and cold temperature T_c, respectively. Different from electronic semiconductive TE material, the sign of S in an ionic system is determined by the type of charge with higher thermal mobility in the solution.[3] Therefore, the transportations of ions under a temperature gradient, which is also known as the Soret effect, should be the key points to determine the thermopower of the ionic system. For most cases, the temperature gradient drives the ions moving from the hot region towards the cold region. Meanwhile, the mass diffusion process also drives the ions from a high-concentration region towards low concentration region. Hence a concentration gradient will be created under these two effects.[36] In addition, the diffusion process can also be taken as the ions in the system are driven by forces with diverse directions, namely, the driving forces from the temperature and ion concentration gradient, respectively. At the final steady state, both the cations and anions in the i-TE system should have higher ion concentrations at low-temperature region than that of high-temperature region and the thermopower should be determined by the concentration differences between the cations and anions at both ends.

Onsager's theory for irreversible processes provides a good framework for understanding of the ion's motions.[37,38] In the system with two current flow (heat and mass) and each of them can be driven by the other, the current of each flow can be expressed by Onsager's theory and the current J_i of the solute species (or ions) i can be expressed as:

$$J_i = -L_{ii}\frac{1}{T}\nabla\mu - L_{iq}\nabla\frac{1}{T} \quad (1)$$

where the first term describes Fick diffusion (or mass diffusion) with coefficient L_{ii} and the second one describes the thermodiffusion with the Onsager cross coefficient L_{iq}[39] Different from simple chemical system, the potential term μ in this system consists of both chemical potential and electrical potential, which can be regarded as the electrochemical potential.[40] The coefficient L_{ii}, L_{iq} can be obtained from experiments and theories. After the illustration and simplifications (refer to derivation in Supporting Information), the thermopower of the ionic system can be expressed as:

$$S_{td} = \frac{n_+D_+\hat{S}_+ - n_-D_-\hat{S}_-}{e(n_+D_+ + n_-D_-)} \quad (2)$$

where e is charge of electron, n is the concentration of the ion, D is mass diffusion coefficient, $\hat{S}$ is the Eastman entropy of transfer and the sign "+" and "-" represents for the cations and anions, respectively. Similar to the Einstein's relation for diffusion driven by a concentration gradient, the diffusion driven by temperature gradient can also has a thermal mobility which is defined as $D\hat{S}/k_BT$.[3] The Eastman entropy of transfer is directly related to the heat of transport Q^*, which has dependence on the size of ions and dielectric constant of the solutes by Born theory.[25,41,42] In the case of a symmetrical electrolyte like LiCl with ($n_+ = n_-$), Equation (2) can be simplified.

We studied three scenarios of the transportations of both cations and anions in an i-TE system, that is, before, during and after the phase-transition. Let us consider **the first scenario** of homogenous electrolyte solution without the phase transition under a temperature gradient. **Figure 2a(i)** illustrates the transportations of both cations and anions in a homogenous liquid-state electrolytes, which expresses the i-TE system before phase-transition. The diffusion coefficient of the cations and anions can be taken as a constant with the temperature change. Meanwhile, both the cations and anions can move fluently in water-based solution without phase-transition, which means the differences between the diffusion coefficient of cations and anions can be neglectable when analysis the thermodiffusion effect in aqueous solutions compared with the thermodiffusion effect in high viscous solutions. These conditions can be expressed as: $n_+ = n_-$ and $D_+ \approx D_-$

Therefore, by taking those condition into consideration, the thermopower of the ionic system for symmetrical electrolyte without phase transition can be roughly simplified into:

$$S_{td} = \frac{\hat{S}_+ - \hat{S}_-}{2e} \quad (3)$$

From this equation, it can be clearly observed that in aqueous solutions, the thermopower of the symmetrical electrolyte mainly depends on the heat of transport of the ions during the moving process, which has been confirmed from the previous research that the heat of transport of Li^+ is larger than that of Cl^- in aqueous solutions.[43] This result is also in good agreement with experiment results that the thermopower of this system is positive.

In **the second scenario**, comparing with the liquid-state system, the motions of ions in gel-state system or viscous system are quite different. **Figure 2a(ii)** illustrates the transportations of both cations and anions in a homogenous gel-state electrolytes, which expresses the i-TE system after phase-transition. As temperature increases, the poloxamer 407 molecules tend to form a net grid, which result in a gel-state of the

solution and increase the viscosity. In viscous system, due to the size difference of the anions and cations, the diffusion coefficient of the ions could be different from each other. We can still neglect the change of diffusion coefficient under temperature gradient in homogenous system without phase transition and the conditions in this case can be expressed as:

$n_+ = n_-$ and $D_+ \neq D_-$

Then the equation (2) can be simplified into:

$$S_{td} = \frac{D_+\hat{S}_+ - D_-\hat{S}_-}{e(D_+ + D_-)} \quad (4)$$

To further simplify this equation, we can take the diffusion coefficient of anions as a reference constant and the value of the cations as a certain ratio k to that of anions. Then Equation (4) can be simplified into:

$$S_{td} = \frac{k\hat{S}_+ - \hat{S}_-}{(1+k)e} \quad (5)$$

Previous research pointed out the proportional relations between the heat of transport and hydration energy[44–46], which means the comparing with the heat of transport, the difference of diffusion coefficient between the anions and cations could be an important factor to determine the increase or decrease of the thermopower compared with value in liquid-state system. In this system, the diffusion coefficient differences between the cations and anions are slightly decreased as the phase changes from liquid-state to gel-state, which makes the k value in gel-state larger than that in liquid-state. This prediction is also in good agreement with the result that the thermopower of the ionic system in high temperature (gel-state) is slightly larger than that in low temperature (liquid-state).

In **the third scenario**, during the phase-transition temperature range, the whole system exhibits a quasi-gel-sol-state, in which the low temperature region is in liquid-state while the high temperature region in gel-state. **Figure 2a(iii)** illustrates the motions of both cations and anions in quasi-liquid-gel-state electrolytes. In this case, the diffusion coefficient of both the anions and cations cannot be taken as a constant. If we still ignore the change of diffusion coefficient by change of temperature and consider ions in different regions (or ions with different diffusion coefficient cause by phase-transition) as different ions with different diffusion coefficients, Equation (2) can be rewritten into another form as:

$$S_{td} = \frac{\sum \hat{S}_+ n_+ D_+ - \sum \hat{S}_- n_- D_-}{e(\sum n_+ D_+ + \sum n_- D_-)} \quad (6)$$

Phase transition, however, is a quite complicated process which is quite difficult to

describe geometrically in this system. Therefore, we cannot set the model which can geometrically describe the boundary of each phase. To solve this problem, we can take the ions moving in different phases as ions with different diffusion coefficients and Eastman entropy of transfer. Then sigma symbol in Eq. 6 can be expressed as the sum value of both cations and anions with different diffusion coefficient and Eastman entropy of transfer. In quasi-gel-liquid-state system, the diffusion coefficient of the ions will change as the environment changes. However, due to the complexity of the phase-transition process, the quantitative description about the diffusion coefficient in the whole system is quite difficult to achieve. Therefore, we define the ratio of thermopower during and before the phase transition (γ) as a function of six dimensionless parameters, that is, ratios of concentrations of cations (a_+) and anions (a_-) at cold ends to total concentration, ratios of diffusion coefficients of cations (b_+) and anions (b_-) in gel-state to that in liquid-state, ratios of diffusion coefficients of cations to anions (k) in liquid-state and ratio of Eastman entropy of cations to anions (l) . **Supplementary Information** provides a detailed derivation. The thermopower ratio is derived as

$$\gamma = \frac{(((1-a_+)b_+ + a_+)kl - ((1-a_-)b_- + a_-))(k+1)}{(((1-a_+)b_+ + a_+)k + ((1-a_-)b_- + a_-))(kl-1)} \quad (7)$$

We analyze the factors that may affect the thermopower ratio during phase-transition and find out the relations between the ratio γ (the ratio of thermopower during transition to before transition) and the factors. **Figure 2b, c** and **d** show the result by controlling several factors as constant and find out the relations by changing other factors. **Figure 2b** points out the relations between the ratio γ and concentration distribution of cations and anions. During the phase-transition, a rather high thermopower can be reached when the cations and anions are mainly distributed at different ends, which means the cations mainly distribute at cold ends while anions mainly distribute at hot ends could strongly enlarge the thermopower of the system. **Figure 2c** points out the relations between the ratio γ and decrease of diffusion coefficient for ions in gel-state regions. The transportations of ions in gel-state regions are affected and the diffusion coefficient of ions will decrease. However, the ratio γ is weakly affected by the decrease of diffusion coefficient, especially when the diffusion coefficient is low (less than 0.01). **Figure 2d** shows by choosing proper k and l pairs, the ratio γ can achieve peak values of more than 1000, that is, a gigantic change in thermopower three orders of magnitude higher than that in non-transitional state. Meanwhile, the peak values do not distribute regularly with k and l pairs, which is in good agreement with the discussion in supplemental information about the partial derivatives of γ to k. The result shows the

thermopower during the phase-transition may increase by 10-1000 times from that before the phase-transition if choosing k and l values. **Figure 2e** illustrates the ratio γ with respect to the k and l values in more details. The result shows that the γ ratio can be enlarged in several orders when the value kl is close to 1, which indicates the phase-transition effect can become stronger in systems where the differences between Eastman entropy of cations and anions are small or the majority of cations and anions distribute in different ends.

Based on the analysis, we can explain why the thermopower increases by around 6.5 times in the phase-transitional poloxamer/LiCl system. Though the phase-transition decreases the diffusion coefficients of both cations and anions, the large increment of thermopower may slightly be due to the sufficiently small diffusion coefficients (for example, $b_+ < 0.1, b_- < 0.1$). In an i-TE system with fixed k and l values, especially in the system in which the thermal mobility of the cations and anions are quite close to each other ($kl > 1$ and $kl \approx 1$), the increase or even the decrease of thermopower possibly depends on the rearrangement of different ions by the transportations of ions during phase-transition. The phase-transition can strongly affect the transport speed of different ions, which thus changes the distribution of ions. In sol-to-gel phase-transition i-TE system with positive thermopower, the distribution of ions should change from both mainly distribute at cold side (before transition) to cations mainly at cold side and anions mainly at hot side (during transition), which means during the phase transition, $a_+ > 0.5$ and $a_- < 0.5$. Comparing the analysis with **Figure 2b**, we can find out the rearrangement of ions at different ends can possible be the reason of the strong increment of thermopower in LiCl/Poloxamer system, which has also been roughly prove from the experiment result in **Figure S6**.

In the gel-sol phase-transitional LiCl/Agarose system, a sudden decrease of the thermopower can be explained as follows. Similar with the analysis of the LiCl/Poloxamer system, the decrease of diffusion coefficient also has slight effect on the change of thermopower when the diffusion coefficient of both cations and anions in gel-state region are both quite low ($b_+ < 0.1, b_- < 0.1$). In this system, the k and l values are fixed and the change of thermopower depends on the distribution of ions at different ends. However, since this system is a gel-sol phase-transitional system, the cold-side, which is also the gel-state region, should have low diffusion coefficients. Therefore, we can modify Eq.7 to describe this system by changing the meaning of a_- and a_+ to the ratio of concentrations of anions and cations at hot ends to total concentration, respectively. In this system, the limits in this system should change as $0 < a_-, a_+ < 0.5$. Before transition, both the cations and anions have higher

concentrations at the cold end but the cations have larger concentration differences between different ends which result in the positive but rather small thermopower before phase-transition. During the gel-to-liquid phase-transition, both the cations and anions tends to diffuse uniformly and result in the decrease of concentration differences of both ions at different ends, which means a_+ and a_- tend to be close to each other and finally change to a value quite close to 0.5. Based on the analysis, γ in this gel-sol phase-transitional can be less than 1. Therefore, the positive thermopower should experience a sudden decrease during the gel-to-sol phase-transition. We observed both the increase and decrease of thermopower caused by phase-transition but the model predicts a rather gigantic increment of thermopower when the parameters of the i-TE system are suitable. In summary, introducing the phase-transition into an i-TE system can modify the thermopower and gigantic effects can be observed if the system is suitable.

Other transitional i-TE materials: Since the operational principle is universal for i-TE material systems, it is reasonable to hypothesize that phase transitions induced by other means (e.g. pH, light, electric field)[47] than thermal method should have a similar effect on thermopower. Hence, we designed and investigated other i-TE material systems to observe the phase-transition induced great variations of thermopower, namely, light induced transition in UV sensitive gels/LiCl. By exposing the region near the hot end to the UV-light during the measurement of the thermopower, a sudden increasement of thermopower was observed and the increasement of the positive thermopower confirmed that the sol-to-gel phase-transition enhanced the positive thermopower no matter what causes the phase-transition (**Figure 2f and 2g**).

3. Conclusion

We have observed the large effect of sol-gel phase transition on thermopower in three different types of i-TE systems. We firstly reported the huge increasement of thermopower (6.5 folds) and ionic figure of merit ZT_i (23 folds) in poloxamer/LiCl aqueous i-TE system during the thermal-induced phase transition from sol-state to gel-state. A positive thermopower of around 15.4 mV/K has been achieved at around 17.4 ℃ when the phase-transition of the i-TE system started happening. On the contrast, the thermopower sudden dropped for several times in agarose/LiCl aqueous i-TE system during its gel-to-liquid phase-transition. Not limited by thermally induced phase-transition, UV-sensitive epoxy/LiCl system also experienced a rapid change of thermopower due to the phase change caused by UV induced cross-linking of polymer network. We revealed the mechanism and proposed a model describing the

thermopower and transportation of ions in the pre-, post- and during-transition stages. From present theoretical results, we confirmed that the large phase-transition-induced thermopower phenomenon is universal regardless the type of causes for the sol-gel phase transition. Our findings open a novel and feasible route to modify the thermoelectric performances of i-TE materials by controlled phase-transition for future tunable i-TE devices in low-heat energy harvesting applications.

4. Experimental Section

Materials.

LiCl (Dieckmann, ≥ 99.0%), NaCl (Dieckmann, ≥ 99.0%), KCl (Dieckmann, ≥ 99.0%), KNO_3 (Dieckmann, ≥ 99.0%), oxirane, methyl-, polymer with oxirane (Poloxamer 407, Sigma, purified, non-ionic), acrylic formulation (PolyJet Photopolymer, RGD810, Veroclear) were purchased and used without any further purification.

Preparation of the i-TE liquids and test cells.

Details about the mass of components and volumes of liquids for the four i-TE systems are listed in **Table 1**. We prepared the poloxamer 407 i-TE liquids of various concentrations by using the same procedures except for the differences on mass of each component. The first step was to mix the poloxamer 407 with water to prepare the basic aqueous solution of poloxamer 407 for a given concentration. Then the poloxamer 407 aqueous solution was kept at 4℃ for more than 12 hours to make sure the polymer was completely dissolved. Then we took a given amount of LiCl and dissolved it into a given volume of prepared poloxamer 407 solution. The mixture was kept at 4℃ for more than 2 hours. The i-TE liquids were ready for further characterizations after these treatments. This LiCl/poloxamer 407 had a sol-to-gel phase transition in the experimental temperatures range from 15℃ to 20℃. We also prepared the agarose-based i-TE liquids with similar procedures and the only difference was the liquid needed to be kept at high temperature (larger than 50℃) to make sure the LiCl was totally dissolved. This system has a gel-to-sol phase transition from 25℃ to 30℃. The UV-sensitive-gel-based i-TE liquids were prepared by same procedure except the whole preparation was kept in non-UV-light environments and the salt was directly dissolved into the UV-sensitive-gel without any other treatments.

We made test cells containing the i-TE liquids inside with two electrodes connected to two ends of the cell, as shown in **Figure 1a**. The test cells were set with the same size (outer diameter of 20mm, thickness of around 1mm) and the electrodes were also

controlled with the same size (side length 30mm, thickness 0.5mm, square shape). The experimental set-up of the test cells is shown in **Figure 1b**. We adhered one piece of the carbon electrode onto the PMMA frame by using glues (Fast-setting epoxy adhesive, AB type, Arlaoda) and then filled in the prepared poloxamer-based or UV-sensitive-gel-based i-TE liquids. After filled in the liquids, we adhered another piece of carbon electrode onto the other side of the PMMA frame with the same way and sealed the whole adhered regions with glues to avoid the leakage of the liquids. The preparation of the agarose-based i-TE cells followed the same procedures except the liquids were heated up to 60℃ before poured into the test cells. The preparation of the UV-sensitive-gel-based i-TE cells followed the same procedures except the preparation was kept in non-UV-light environments.

Characterizations and measurements.

Thermopower: The thermopower, or ionic Seebeck coefficient**,** electrical properties and temperature differences were measured simultaneously by using a thermocouple thermometer and electrochemical workstation together. The experimental set-ups are shown in **Figure S1 of Supplementary Information**. The test cells were placed between two planar metal plates, which provided the temperature difference monitored by the thermocouples. The electric voltage induced by different ΔT values were obtained from 5℃ to 35℃, by changing the temperature of both the hot side and cold side together. In this work, we set the temperature differences between the hot side and cold side as a fixed value of 3 K. The ratio of the measured open-circuit voltage difference to the temperature difference was taken as the thermopower at the temperature of the cold side. We repeated the measurements for 5-7 times at each temperature point and the thermopower was taken from the average value of the maximum and the minimum readings. The voltage difference was measured by an electrochemical workstation (CHI660E, CH Instrument, USA) in open-circuit voltage mode and the temperature difference was provided by a self-made heating and cooling plates with temperature controller. The temperature of the hot side and cold side of the TEG was monitored real-time by a thermocouple thermometer (Anbat AT4516).

Electrical conductivity: The ionic electrical conductivity was characterized by a standard method established for electrochemical devices.[48] The complex electrical impedance of the TE materials was measured by the electrochemical workstation (CHI660E, CH Instrument, USA) in electrical impedance spectroscopy (EIS) mode. The setting input voltage was related to the measured open-circuit voltage and the measured frequency range was from 10^{5}~10^{-2} Hz (small differences for different materials). The electrical

conductivity was calculated from the real part of the impedance at phase angle close to 0° in the Nyquist plot measured by the EIS as:

$$\sigma = \frac{L}{Z'A}$$

where Z' is the measured real part of the impedance, L and A are the length and area of the test TEG, respectively.

Cyclic voltammetry (CV) curves: The cyclic voltammetry (CV) curves were measured to determine the working mode (capacitive or not) of the target TE materials. The CV curves was also measured by CHI660E, (CH Instrument, USA) in I-V curve mode. The scanning rate was 10 mV/s and the scanning voltage was set from 0V to 0.4V. All the electrical and thermoelectric characterizations were conducted on the test cells with the same configuration and same size.

Thermal conductivity: Thermal conductivity was measured by using Thermal Conductivity Measurement Instrument (Hotdisk, TPS2500s) for liquid-state samples. The experiments were conducted at room temperature.

***Output power*:** We set the temperature differences between the different sides of the i-TE cells as 3K and connected the external resistance load to the i-TE cells when the output voltage of the cell is stable. The maximum output power of the i-TE system was chosen by the maximum value of the voltage across the resistance times current through the it.

Viscosity of the sol-gel systems: The viscosity of the samples was measured by Brookfield DV2T viscometer (AMETEK Brookfield, US) with the shear rate of 200 r/s. The used spindle number was 5. We poured the 20 mL of the liquid-state samples into the 50mL breaker and put the break into a larger 200mL breaker with ice and water inside to measure the temperature dependence viscosity. The temperature during the measurements was controlled by heating the larger breaker and monitored by the thermometer inserted.

Acknowledgements

The work has been partially supported by Research Grants Council, Hong Kong (Grant. No. 15202020E, 15201419E, 15200917E), Hong Kong Polytechnic University (Grant No. 847A), National Natural Science Foundation of China (Grant No. 52073066) and the GDAS Project of Science and Technology Development (Grant No. 2020GDASYL-20200102028). L.J. thanks The Hong Kong Polytechnic University for a postgraduate

scholarship. The authors thank Dr. Lin Shuping for conducting viscosity measurements.

Conflict of Interest

The authors declare no conflict of interest.

Data Availability Statement

The data that support the findings of this study are available from the corresponding authors upon reasonable request.

References:

(1) Li, X.; Cai, K.; Gao, M.; Du, Y.; Shen, S. Recent Advances in Flexible Thermoelectric Films and Devices. *Nano Energy* **2021**, *89*, 106309. https://doi.org/10.1016/J.NANOEN.2021.106309.

(2) Haras, M.; Skotnicki, T. Thermoelectricity for IoT – A Review. *Nano Energy* **2018**, *54*, 461–476. https://doi.org/10.1016/J.NANOEN.2018.10.013.

(3) Han, C. G.; Qian, X.; Li, Q.; Deng, B.; Zhu, Y.; Han, Z.; Zhang, W.; Wang, W.; Feng, S. P.; Chen, G.; Liu, W. Giant Thermopower of Ionic Gelatin near Room Temperature. *Science (80-.).* **2020**, *368* (6495), 1091–1098. https://doi.org/10.1126/science.aaz5045.

(4) He, J.; Tritt, T. M. Advances in Thermoelectric Materials Research: Looking Back and Moving Forward. *Science (80-.).* **2017**, *357* (6358). https://doi.org/10.1126/SCIENCE.AAK9997/ASSET/8273CBC8-7739-44FF-A41C-5530E2BBF995/ASSETS/GRAPHIC/357_AAK9997_F6.JPEG.

(5) Vining, C. B. An Inconvenient Truth about Thermoelectrics. *Nat. Mater. 2009 82* **2009**, *8* (2), 83–85. https://doi.org/10.1038/nmat2361.

(6) Zhang, Q.; Liao, B.; Lan, Y.; Lukas, K.; Liu, W.; Esfarjani, K.; Opeil, C.; Broido, D.; Chen, G.; Ren, Z. High Thermoelectric Performance by Resonant Dopant Indium in Nanostructured SnTe. *Proc. Natl. Acad. Sci. U. S. A.* **2013**, *110* (33), 13261–13266. https://doi.org/10.1073/PNAS.1305735110/SUPPL_FILE/PNAS.201305735SI.PDF.

(7) Zhao, L. D.; Lo, S. H.; Zhang, Y.; Sun, H.; Tan, G.; Uher, C.; Wolverton, C.; Dravid, V. P.; Kanatzidis, M. G. Ultralow Thermal Conductivity and High Thermoelectric Figure of Merit in SnSe Crystals. *Nature* **2014**, *508* (7496), 373–377. https://doi.org/10.1038/nature13184.

(8) Heremans, J. P.; Jovovic, V.; Toberer, E. S.; Saramat, A.; Kurosaki, K.; Charoenphakdee, A.; Yamanaka, S.; Snyder, G. J. Enhancement of Thermoelectric Efficiency in PbTe by Distortion of the Electronic Density of States. *Science (80-.).* **2008**, *321* (5888), 554–557. https://doi.org/10.1126/SCIENCE.1159725/SUPPL_FILE/HEREMANS_SOM.PDF.

(9) Byeon, D.; Sobota, R.; Delime-Codrin, K.; Choi, S.; Hirata, K.; Adachi, M.; Kiyama, M.; Matsuura, T.; Yamamoto, Y.; Matsunami, M.; Takeuchi, T. Discovery of Colossal Seebeck Effect in Metallic Cu2Se. *Nat. Commun. 2019 101* **2019**, *10* (1), 1–7. https://doi.org/10.1038/s41467-018-07877-5.

(10) Yang, D.; Su, X.; Li, J.; Bai, H.; Wang, S.; Li, Z.; Tang, H.; Tang, K.; Luo, T.; Yan, Y.; Wu, J.; Yang, J.; Zhang, Q.; Uher, C.; Kanatzidis, M. G.; Tang, X. Blocking Ion Migration Stabilizes the High Thermoelectric Performance in Cu2Se Composites. *Adv. Mater.* **2020**, *32* (40), 2003730. https://doi.org/10.1002/ADMA.202003730.

(11) Bai, H.; Su, X.; Yang, D.; Zhang, Q.; Tan, G.; Uher, C.; Tang, X.; Wu, J. An Instant Change of Elastic Lattice Strain during Cu2Se Phase Transition: Origin of Abnormal Thermoelectric Properties. *Adv. Funct. Mater.* **2021**. https://doi.org/10.1002/adfm.202100431.

(12) Chen, C.; Feng, Z.; Yao, H.; Cao, F.; Lei, B. H.; Wang, Y.; Chen, Y.; Singh, D. J.; Zhang, Q. Intrinsic Nanostructure Induced Ultralow Thermal Conductivity Yields Enhanced Thermoelectric Performance in Zintl Phase Eu2ZnSb2. *Nat. Commun. 2021 121* **2021**, *12* (1), 1–9. https://doi.org/10.1038/s41467-021-25483-w.

(13) Jaziri, N.; Boughamoura, A.; Müller, J.; Mezghani, B.; Tounsi, F.; Ismail, M. A Comprehensive Review of Thermoelectric Generators: Technologies and Common Applications. *Energy Reports* **2020**, *6*, 264–287. https://doi.org/10.1016/j.egyr.2019.12.011.

(14) Iezzi, B.; Ankireddy, K.; Twiddy, J.; Losego, M. D.; Jur, J. S. Printed, Metallic Thermoelectric Generators Integrated with Pipe Insulation for Powering Wireless Sensors. *Appl. Energy* **2017**, *208*, 758–765. https://doi.org/10.1016/j.apenergy.2017.09.073.

(15) Cutler, M.; Mott, N. F. Observation of Anderson Localization in an Electron Gas. *Phys. Rev.* **1969**, *181* (3), 1336–1340. https://doi.org/10.1103/PhysRev.181.1336.

(16) Kim, H. S.; Gibbs, Z. M.; Tang, Y.; Wang, H.; Snyder, G. J. Characterization of Lorenz Number with Seebeck Coefficient Measurement. *APL Mater.* **2015**, *3* (4), 1–6. https://doi.org/10.1063/1.4908244.

(17) Liu, W.; Tan, X.; Yin, K.; Liu, H.; Tang, X.; Shi, J.; Zhang, Q.; Uher, C. Convergence of Conduction Bands as a Means of Enhancing Thermoelectric Performance of N-Type Mg 2Si 1-XSn x Solid Solutions. *Phys. Rev. Lett.* **2012**, *108* (16), 166601. https://doi.org/10.1103/PHYSREVLETT.108.166601/FIGURES/3/MEDIUM.

(18) Xiao, Y.; Wu, H.; Cui, J.; Wang, D.; Fu, L.; Zhang, Y.; Chen, Y.; He, J.; Pennycook, S. J.; Zhao, L. D. Realizing High Performance N-Type PbTe by Synergistically Optimizing Effective Mass and Carrier Mobility and Suppressing Bipolar Thermal Conductivity. *Energy Environ. Sci.* **2018**, *11* (9), 2486–2495. https://doi.org/10.1039/C8EE01151F.

(19) Zhao, D.; Wang, H.; Khan, Z. U.; Chen, J. C.; Gabrielsson, R.; Jonsson, M. P.; Berggren, M.; Crispin, X. Ionic Thermoelectric Supercapacitors. *Energy Environ. Sci.* **2016**, *9* (4), 1450–1457. https://doi.org/10.1039/c6ee00121a.

(20) Yu, B.; Duan, J.; Cong, H.; Xie, W.; Liu, R.; Zhuang, X.; Wang, H.; Qi, B.; Xu, M.; Wang, Z. L.; Zhou, J. Thermosensitive Crystallization-Boosted Liquid Thermocells for Low-Grade Heat Harvesting. *Science (80-.).* **2020**, *370* (6514), 342–346. https://doi.org/10.1126/science.abd6749.

(21) Cheng, H.; He, X.; Fan, Z.; Ouyang, J. Flexible Quasi-Solid State Ionogels with Remarkable Seebeck Coefficient and High Thermoelectric Properties. *Adv. Energy Mater.* **2019**, *9* (32), 1901085. https://doi.org/10.1002/AENM.201901085.

(22) Lae Kim, S.; Taisun Lin, H.; Yu, C.; Kim, S. L.; Yu, C.; Lin, H. T. Thermally Chargeable Solid-State Supercapacitor. *Adv. Energy Mater.* **2016**, *6* (18), 1600546. https://doi.org/10.1002/AENM.201600546.

(23) Li, T.; Zhang, X.; Lacey, S. D.; Mi, R.; Zhao, X.; Jiang, F.; Song, J.; Liu, Z.; Chen, G.; Dai, J.; Yao, Y.; Das, S.; Yang, R.; Briber, R. M.; Hu, L. Cellulose Ionic Conductors with High Differential Thermal Voltage for Low-Grade Heat Harvesting. *Nat. Mater.* **2019**, *18* (6), 608–613. https://doi.org/10.1038/s41563-019-0315-6.

(24) Kunitski, M.; Eicke, N.; Huber, P.; Köhler, J.; Zeller, S.; Voigtsberger, J.; Schlott, N.; Henrichs, K.; Sann, H.; Trinter, F.; Schmidt, L. P. H.; Kalinin, A.; Schöffler, M. S.; Jahnke, T.; Lein, M.; Dörner, R. Double-Slit Photoelectron Interference in Strong-Field Ionization of the Neon Dimer. *Nat. Commun. 2019 101* **2019**, *10* (1), 1–7. https://doi.org/10.1038/s41467-018-07882-8.

(25) Eastman, E. D. Theory of the Soret Effect. *J. Am. Chem. Soc.* **1928**, *50* (2), 283–291. https://doi.org/10.1021/ja01389a007.

(26) Leighton, C. Electrolyte-Based Ionic Control of Functional Oxides. *Nat. Mater. 2018 181* **2018**, *18* (1), 13–18. https://doi.org/10.1038/s41563-018-0246-7.

(27) Li, X.; Li, M.; Yang, Q.; Li, H.; Xu, H.; Chai, Z.; Chen, K.; Liu, Z.; Tang, Z.; Ma, L.; Huang, Z.; Dong, B.; Yin, X.; Huang, Q.; Zhi, C. Phase Transition Induced Unusual Electrochemical Performance of V2CTX MXene for Aqueous Zinc Hybrid-Ion Battery. *ACS Nano* **2020**, *14* (1), 541–551. https://doi.org/10.1021/ACSNANO.9B06866/ASSET/IMAGES/MEDIUM/NN9B06866_M001.GIF.

(28) Fakhari, A.; Corcoran, M.; Schwarz, A. Thermogelling Properties of Purified Poloxamer 407. *Heliyon* **2017**, *3* (8), e00390. https://doi.org/10.1016/j.heliyon.2017.e00390.

(29) Dumortier, G.; Grossiord, J. L.; Agnely, F.; Chaumeil, J. C. A Review of Poloxamer 407 Pharmaceutical and Pharmacological Characteristics. *Pharm. Res. 2006 2312* **2006**, *23* (12), 2709–2728. https://doi.org/10.1007/S11095-006-9104-4.

(30) Duan, J.; Feng, G.; Yu, B.; Li, J.; Chen, M.; Yang, P.; Feng, J.; Liu, K.; Zhou, J. Aqueous Thermogalvanic Cells with a High Seebeck Coefficient for Low-Grade Heat Harvest. *Nat. Commun.* **2018**, *9* (1), 1–8. https://doi.org/10.1038/s41467-018-07625-9.

(31) Li, G.; Dong, D.; Hong, G.; Yan, L.; Zhang, X.; Song, W.; Li, G.; Dong, D.; Zhang, X.; Hong, G.; Yan, L.; Song, W. High-Efficiency Cryo-Thermocells Assembled with Anisotropic Holey Graphene Aerogel Electrodes and a Eutectic Redox Electrolyte. *Adv. Mater.* **2019**, *31* (25), 1901403. https://doi.org/10.1002/ADMA.201901403.

(32) Kim, K.; Lee, H. Thermoelectrochemical Cells Based on Li+/Li Redox Couples in LiFSI Glyme Electrolytes. *Phys. Chem. Chem. Phys.* **2018**, *20* (36), 23433–23440. https://doi.org/10.1039/C8CP03155J.

(33) Morita, T.; Narita, T.; Mukai, S. A.; Yanagisawa, M.; Tokita, M. Phase Behaviors of Agarose Gel. *AIP Adv.* **2013**, *3* (4), 042128. https://doi.org/10.1063/1.4802968.

(34) Wang, H.; Zhao, D.; Khan, Z. U.; Puzinas, S.; Jonsson, M. P.; Berggren, M.; Crispin, X. Ionic Thermoelectric Figure of Merit for Charging of Supercapacitors. *Adv. Electron. Mater.* **2017**, *3* (4), 1700013. https://doi.org/10.1002/AELM.201700013.

(35) Liu, Z.; Cheng, H.; Le, Q.; Chen, R.; Li, J.; Ouyang, J. Giant Thermoelectric Properties of Ionogels with Cationic Doping. *Adv. Energy Mater.* **2022**, *12* (22), 2200858. https://doi.org/10.1002/AENM.202200858.

(36) Hemmat Esfe, M.; Esfandeh, S.; Kamyab, M. H. History and Introduction. *Hybrid Nanofluids Convect. Heat Transf.* **2020**, 1–48. https://doi.org/10.1016/B978-0-12-819280-1.00001-X.

(37) Onsager, L. Reciprocal Relations in Irreversible Processes. I. *Phys. Rev.* **1931**, *37* (4), 405. https://doi.org/10.1103/PhysRev.37.405.

(38) Onsager, L. Reciprocal Relations in Irreversible Processes. II. *Phys. Rev.* **1931**, *38* (12), 2265. https://doi.org/10.1103/PhysRev.38.2265.

(39) Non-Equilibrium Thermodynamics - S. R. De Groot, P. Mazur - Google Books https://books.google.com.hk/books?hl=en&lr=&id=mfFyG9jfaMYC&oi=fnd&pg=PP1&ots=ih_gwuGYmt&sig=d8RgYKq33Wds2o2zBCDI3Ve41mI&redir_esc=y#v=onepage&q&f=false (accessed Dec 23, 2021).

(40) Huang, B. T.; Roger, M.; Bonetti, M.; Salez, T. J.; Wiertel-Gasquet, C.; Dubois, E.; Cabreira Gomes, R.; Demouchy, G.; Mériguet, G.; Peyre, V.; Kouyaté, M.; Filomeno, C. L.; Depeyrot, J.; Tourinho, F. A.; Perzynski, R.; Nakamae, S. Thermoelectricity and Thermodiffusion in Charged Colloids. *J. Chem. Phys.* **2015**, *143* (5), 054902. https://doi.org/10.1063/1.4927665.

(41) Agar, J. N.; Mou, C. Y.; Lin, J. L. Single-Ion Heat of Transport in Electrolyte Solutions: A Hydrodynamic Theory. *J. Phys. Chem.* **2002**, *93* (5), 2079–2082. https://doi.org/10.1021/J100342A073.

(42) Eastman, E. D.; 48, Y. THERMODYNAMICS OF NON-ISOTHERMAL SYSTEMS. *J. Am. Chem. Soc.* **2002**, *48* (6), 1482–1493. https://doi.org/10.1021/JA01417A004.

(43) Di Lecce, S.; Albrecht, T.; Bresme, F. A Computational Approach to Calculate the Heat of Transport of Aqueous Solutions. *Sci. Reports 2017 71* **2017**, *7* (1), 1–10. https://doi.org/10.1038/srep44833.

(44) Rezende Franco, L.; Sehnem, A. L.; Figueiredo Neto, A. M.; Coutinho, K. Molecular Dynamics Approach to Calculate the Thermodiffusion (Soret and Seebeck) Coefficients of Salts in Aqueous Solutions. *J. Chem. Theory Comput.* **2021**, *17* (6), 3539–3553. https://doi.org/10.1021/ACS.JCTC.1C00116/SUPPL_FILE/CT1C00116_SI_001.PDF.

(45) Takeyama, N.; Nakashima, K. Proportionality of Intrinsic Heat of Transport to Standard Entropy of Hydration for Aqueous Ions. *J. Solut. Chem. 1988 174* **1988**, *17* (4), 305–325. https://doi.org/10.1007/BF00650412.

(46) Burgess, J. Ion–Solvent Interactions. *Ions Solut.* **1999**, 45–61. https://doi.org/10.1533/9781782420569.45.

(47) Swift, T.; Swanson, L.; Geoghegan, M.; Rimmer, S. The PH-Responsive Behaviour of Poly(Acrylic Acid) in Aqueous Solution Is Dependent on Molar Mass. *Soft Matter* **2016**, *12* (9), 2542–2549. https://doi.org/10.1039/C5SM02693H.

(48) Akgöl, Y.; Cramer, C.; Hofmann, C.; Karatas, Y.; Wiemhöfer, H. D.;

Schönhoff, M. Humidity-Dependent Dc Conductivity of Polyelectrolyte Multilayers: Protons or Other Small Ions as Charge Carriers? *Macromolecules* **2010**, *43* (17), 7282–7287. https://doi.org/10.1021/MA1012489/ASSET/IMAGES/MEDIUM/MA-2010-012489_0004.GIF.

Table 1 Details of i-TE systems

I-TE solutions	Mass of salts	Mass of polymer	Volume of water	Volume of gel
10%Polo+ 1 M/L LiCl	0.05 mol (2.12g)	20g	200 mL	50 mL
18%Polo+ 1 M/L LiCl	0.05 mol (2.12g)	36g	200 mL	50 mL
20%Polo+ 1 M/L LiCl	0.05 mol (2.12g)	40g	200 mL	50 mL
2% Agarose + 1M/L LiCl	0.05 mol (2.12g)	4g	200 mL	50 mL
UV-sensitive-gel-based	0.006 mol (0.254g)	NIL	NIL	20 mL

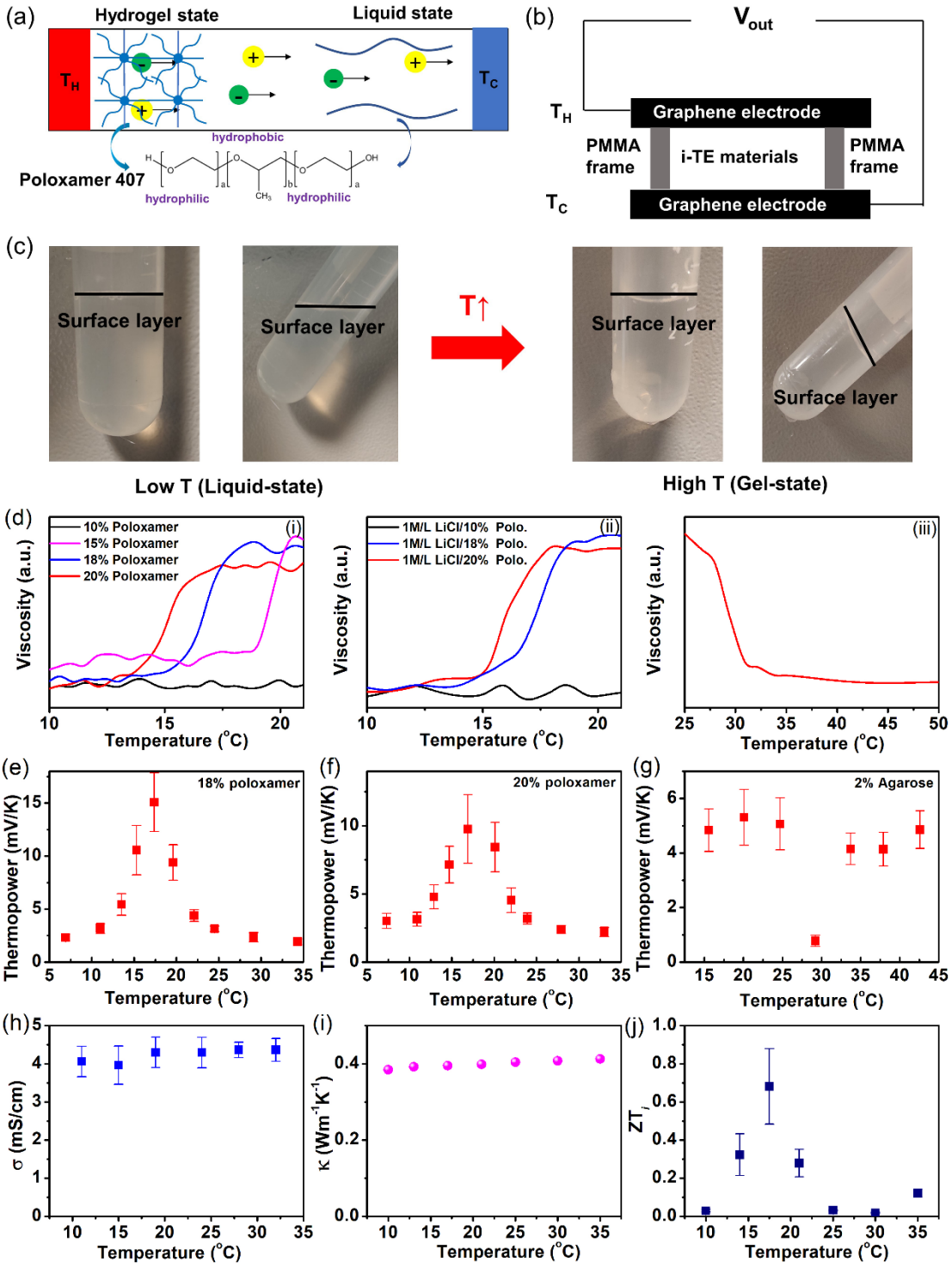

Figure 1 Schematic illustrations of the i-TE system and characterizations of the system. a. Schematics of the components of the i-TE materials in the thermoelectric cell. **b.** Schematics of the thermoelectric cell prepared for the measurements of the thermoelectric performances. **c.** Liquid-to-gel phase transition of LiCl/poloxamer 407 solution. The surface layer of the solution is marked and labeled by thick black line from the figure. At low temperature, the solution surface of the declined tube is level. The surface of the gel is not level at high temperature. **d.** Viscosity of various ionic sol-

gel systems: **i).** Viscosity of poloxamer 407 aqueous solutions with different concentrations. **ii).** Viscosity of the ionic system with 1 mol/L LiCl in 10%, 18% and 20% (w/v) poloxamer aqueous solutions. **iii).** Viscosity of the 2% (w/v) agarose-based 1 mol/L LiCl ionic solution. **e.** Thermopower-temperature relationship of the 18% (w/v) poloxamer 407-based 1 mol/L LiCl ionic solution. **f.** Thermopower-temperature relationship of the 20% (w/v) poloxamer 407-based 1 mol/L LiCl ionic solution. **g.** Thermopower-temperature relationship of the 2% (w/v) Agarose-based 1 mol/L LiCl ionic solution. **h.** Electrical conductivity of 18% (w/v) poloxamer 407-based 1 mol/L LiCl ionic solution. The electrical conductivity was obtained from the electrical impedance spectroscopy. **i.** Thermal conductivity of the 18% (w/v) poloxamer 407-based 1 mol/L LiCl ionic solution. **j.** Ionic figure of merit ZT_i of the 18% (w/v) poloxamer 407-based 1 mol/L LiCl ionic solution at different temperature.

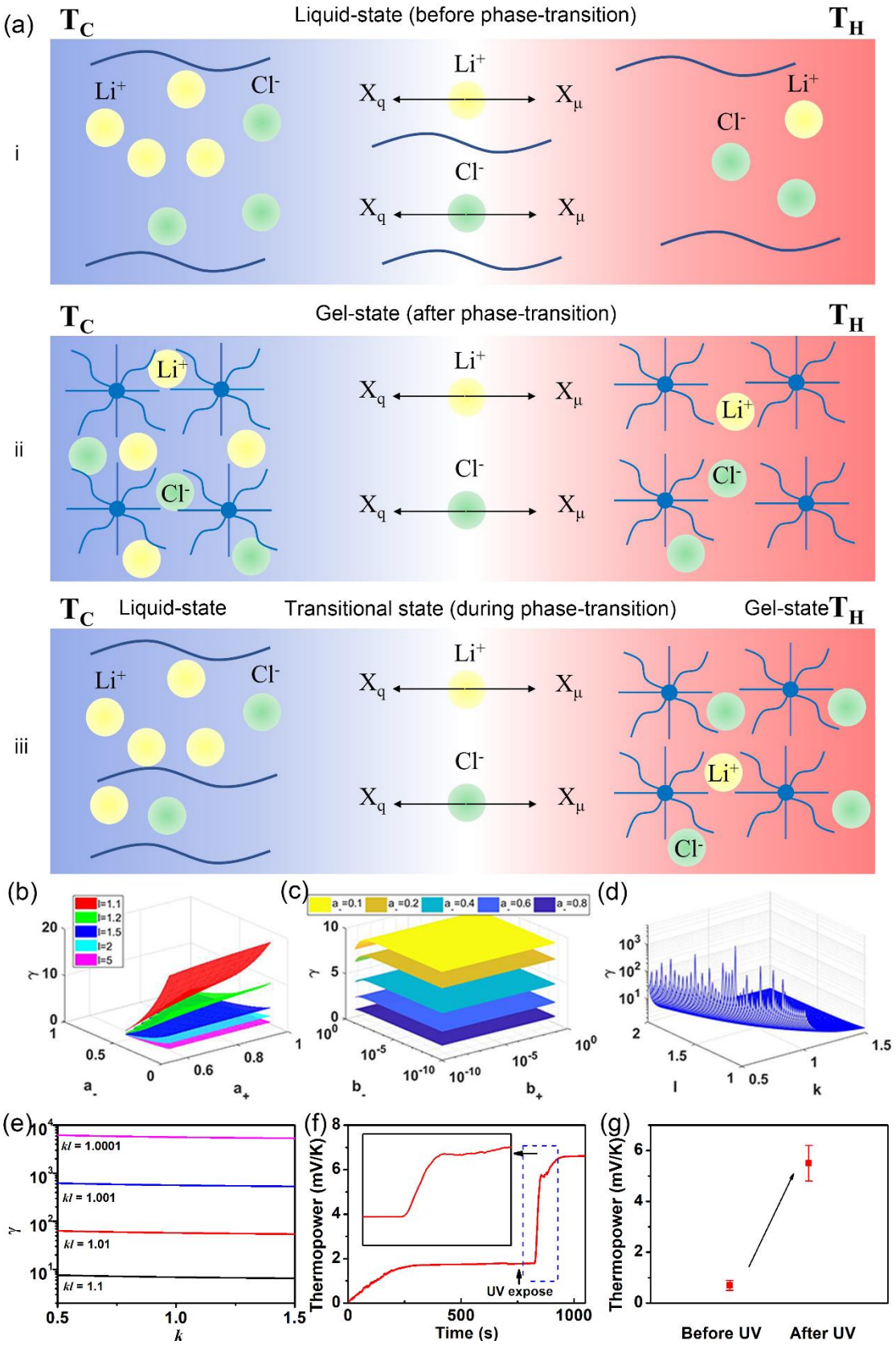

Figure 2 Mechanism and other transitional i-TE materials. a. Schematic of the diffusion process of cations and anions under a temperature gradient within transitional i-TE system in (i) liquid-state (before phase-transition) (ii) gel-state (after phase-

transition) and (iii) quasi-state (during phase-transition). The blue lines represent the structure of the poloxamer, which indicate the phase of the system. The driven forces X_q and X_μ are from temperature gradients and electrochemical potential, respectively. **b.** γ plotted as a function of a_+ , a_- and l with other fixed (k = 1, b_- = b_+ = 0.01). **c.** γ plotted as a function of b_+, b_- and a_- with others fixed (a_+ = 0.9, k = 1, l = 1.2). **d.** γ plotted against of k and l with others fixed (b_+ = b_- = 0.01, a_+ = 0.9, a_- = 0.5). **e.** γ plotted against of k with others fixed (b_+ = b_- = 0.01, a_+ = 0.9, a_- = 0.5, kl equals to different constants as labeled in figure). **f.** Output open-circuit voltage of the UV sensitive gel-based 0.3 M/L LiCl solution before and after UV exposure to the high-temperature region. The temperature is set for 15℃ at cold side and 18℃ at hot side. **g.** Output thermopower before and after UV light exposure for this system.